PHYSICAL REVIEW B **96**, 020501(R) (2017)

Observation of the Bloch-Siegert shift in a driven quantum-to-classical transition

I. Pietikäinen,[1] S. Danilin,[2] K. S. Kumar,[2] A. Vepsäläinen,[2] D. S. Golubev,[2] J. Tuorila,[1,3] and G. S. Paraoanu[2,*]

[1]*Nano and Molecular Materials Research Unit, University of Oulu, P.O. Box 3000, FI-90014 Oulu, Finland*

[2]*Centre for Quantum Engineering and LTQ, Department of Applied Physics, Aalto University, P.O. Box 15100, FI-00076 Aalto, Finland*

[3]*COMP Centre of Excellence, Department of Applied Physics, Aalto University, P.O. Box 15100, FI-00076 Aalto, Finland*

(Received 9 December 2016; published 7 July 2017)

We show that the counter-rotating terms of the dispersive qubit-cavity Rabi model can produce relatively large and nonmonotonic Bloch-Siegert shifts in the cavity frequency as the system is driven through a quantum-to-classical transition. Using a weak microwave probe tone, we demonstrate experimentally this effect by monitoring the resonance frequency of a microwave cavity coupled to a transmon and driven by a microwave field with varying power. In the weakly driven regime (quantum phase), the Bloch-Siegert shift appears as a small constant frequency shift, while for a strong drive (classical phase) it presents an oscillatory behavior as a function of the number of photons in the cavity. The experimental results are in agreement with numerical simulations based on the quasienergy spectrum.

DOI: 10.1103/PhysRevB.96.020501

The Rabi Hamiltonian—describing a two-level system coupled to a cavity (resonator) mode—is a paradigmatic model in quantum physics. In the rotating-wave approximation (RWA) it leads to the well-known Jaynes-Cummings (JC) model. In the dispersive limit this model predicts the appearance of ac Stark shifts in the energy levels of both the qubit and the cavity. The inclusion of counter-rotating terms produces an additional displacement of the energy levels. This Bloch-Siegert (BS) shift [1] is usually very small on standard experimental platforms since it depends on the ratio between the coupling and the sum of the Larmor and cavity frequencies. Recently, however, significant experimental effort has been put into increasing the coupling to values comparable with the Larmor frequency [2–4], most notable in semiconductor dots [5,6] and superconducting circuits [7–12]. Other approaches for observing the Bloch-Siegert shift include a detailed analysis of two-level Landau-Zener spectra of Rydberg atoms [13,14] and Cooper-pair boxes [15–17], as well as the simulation of the Rabi model in rotating frames [18,19].

In this Rapid Communication we take a different route. We recognize that the counter-rotating terms do not conserve the excitation number. Therefore, the natural framework for their experimental demonstration is that of driven-dissipative systems [20,21]. Guided by this intuition, we realize a setup consisting of a transmon [22] dispersively coupled to a cavity, where the cavity is driven at a fixed off-resonance microwave tone, while at the same time the spectrum is scanned by a comparatively weaker probe field (see Fig. 1). At low driving powers, we observe the expected vacuum ac Stark shift [23–27]. This is followed by a transition regime dominated by nonlinear effects as the power is increased. For the Jaynes-Cummings model, such a transition has been predicted and studied in the resonant qubit-cavity case [28–31]. In the dispersive limit, the transition region is no longer abrupt, but it is expected to soften into a Kerr-type nonlinearity [29], in agreement with our observations.

As the system approaches and enters the classical phase, the frequency renormalization due to the BS effect results in a strongly nonmonotonic dependence on the number of photons in the cavity. The effect escapes the scope of the simple RWA, but can be modeled numerically using the Floquet formalism [32] for a driven cavity coupled with a multilevel transmon. The measured deviation from the RWA result is in agreement with the simulations and constitutes an experimental observation of the BS effect in a driven quantum-to-classical transition.

Theoretical predictions for a two-level system. We develop a simple physical picture of these phenomena by considering the two lowest transmon states coupled with a cavity which is driven by a tone of amplitude A and frequency ω_d. The resulting driven Rabi Hamiltonian (scaled with $\hbar$) is written as

$$\hat{H} = \omega_c \hat{a}^\dagger \hat{a} + \frac{\omega_0}{2}\hat{\sigma}_z + g(\hat{a}^\dagger + \hat{a})\hat{\sigma}_x + A\cos(\omega_d t)(\hat{a}^\dagger + \hat{a}), \tag{1}$$

where ω_c and ω_0 are the frequencies of the cavity and the qubit, respectively, and g is the strength of the coupling (see Fig. 1). We displace the Hamiltonian in Eq. (1) into the vacuum and apply the RWA. After a Schieffer-Wolff transformation, we obtain the driven JC Hamiltonian [33],

$$\hat{H} = (\omega_c + \chi_0\hat{\sigma}_z)\hat{a}^\dagger\hat{a} + \frac{1}{2}(\omega_0 + \chi_0)\hat{\sigma}_z + \frac{G}{2}(e^{i\omega_d t}\hat{\sigma}_- + e^{-i\omega_d t}\hat{\sigma}_+), \tag{2}$$

where $\chi_0 = g^2/(\omega_0 - \omega_c)$ is the vacuum ac Stark shift. Thus, the cavity frequency $\omega_c + \chi_0\hat{\sigma}_z$ depends on the qubit state, which is modulated by a drive with an effective strength $G = gA/\sqrt{(\omega_c - \omega_d)^2 + \kappa^2/4}$, where κ is the cavity dissipation. Consequently, at high powers, the effective cavity frequency becomes a weighted average over the qubit state [18,34], i.e., simply ω_c.

However, G diverges with increasing A, thus we expect that the RWA is not valid at large drive powers. To capture the behavior in this regime, we again transform the cavity in Eq. (1) into the vacuum and then apply the counter-rotating hybridized rotating-wave (CHRW) approximation [35,36]. After a Schrieffer-Wolff transformation, we obtain Eq. (2),

*sorin.paraoanu@aalto.fi

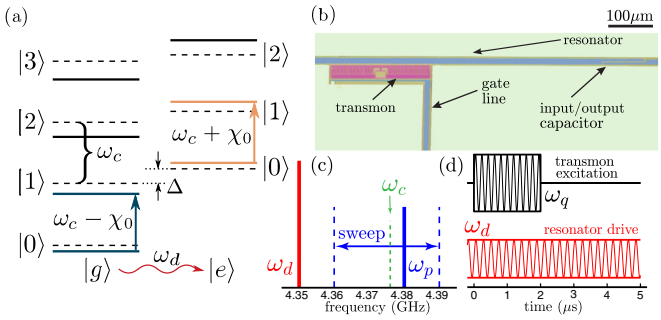

FIG. 1. Schematic of the experimental setup. (a) Energy levels of a dispersive JC system. The vacuum ac Stark shift is given by $\chi_0 = g^2/(\omega_0 - \omega_c)$. (b) Optical micrograph of the main elements of the sample (false colors). (c) We drive the cavity with a detuned drive frequency $\omega_d < \omega_c$. The spectrum of the system is monitored by a weak probe with frequency ω_p, which is swept within the window [4.36,4.39] GHz. (d) In the T_1 measurements, the cavity is driven continuously at ω_d. In the steady state, a long 2 μs microwave pulse at the ac Stark shifted transmon frequency $\omega_q \gg \omega_c$ is applied to the gate line of the transmon. When the pulse ends, the decay traces of the system relaxing back to the steady state are monitored in the time domain using a homodyne detection scheme.

but with a renormalized qubit frequency $\tilde{\omega}_0 \equiv \omega_0 J_0(2G\xi/\omega_d)$ and drive amplitude $\tilde{G}/2 \equiv G(1-\xi)$. The parameter ξ is determined by solving $G(1-\xi) = \omega_0 J_1(2G\xi/\omega_d)$ [33].

We show the effective cavity resonance frequencies in the RWA and CHRW approximation in Fig. 2(a). We compare the results with the numerical simulations [33] of the probe reflection coefficient $\Gamma(\omega_p) = [Z(\omega_p) - Z_0]/[Z(\omega_p) + Z_0]$, where $Z(\omega_p)$ and Z_0 are the impedances of the driven cavity coupled to a two-level transmon and the transmission line, respectively. The impedance $Z(\omega_p)$ was calculated from the probe-induced transition rates between the quasienergy states of the driven cavity-transmon system by employing the Kramers-Kronig relation [17,33,37–44]. We see that the RWA gives an overall qualitative behavior relatively well but lacks the nonmonotonic behavior of the simulated resonance frequency toward the high-power end of the spectrum. The CHRW approximation is nonmonotonic and is quite accurate when compared to the full numerical solution with $G/\omega_d < 1$, and even for higher values of G when $\omega_0/\omega_d < 1$ [35]. However, it still fails to match exactly the average numerical resonance at high drive powers, since it neglects the second and higher harmonics of the drive. At low powers, the deviation between the analytic and numerical resonance locations is caused by the vacuum BS shift $\chi_{BS} = g^2/(\omega_0 + \omega_c) = 2\pi \times 0.7$ MHz. Strong driving clearly amplifies the BS effect, which appears as a deviation of nearly 3 MHz between the RWA and CHRW reflection minima.

From Fig. 2(b) we can see the existence of three regimes: At small average photon numbers, the response of the system is quantum mechanical and corresponds to a cavity with constant frequency shift. When the number of photons becomes of the order of unity, the response is sensitive to the addition or removal of photons, indicating a dispersive photon blockade [45]. At large numbers of photons, the photon blockade breaks [29], and the Bloch-Siegert shift produces an oscillatory response as a function of added photons.

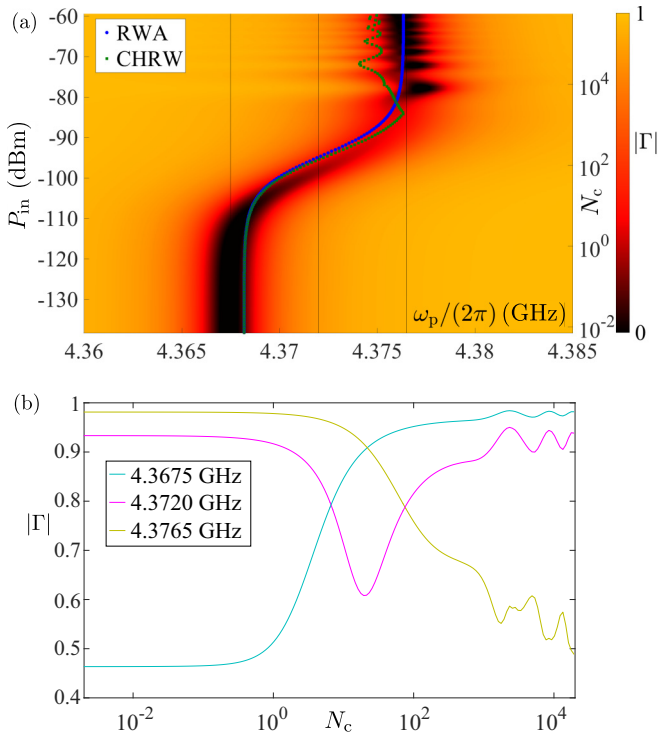

FIG. 2. Numerical simulation of the spectrum for a two-level system, corresponding to experimental values $\omega_c/(2\pi) = 4.376$ GHz, $\omega_0/(2\pi) = 5.16$ GHz, $g/(2\pi) = 80$ MHz, $\omega_d/(2\pi) = 4.350$ GHz, and $\kappa/(2\pi) = 4.0$ MHz. (a) Probe reflection coefficient $|\Gamma|$ as a function of probe frequency ω_p and cavity occupation N_c. The locations of resonance in the RWA (blue) and in the CHRW (green) approximations are shown as well. (b) Reflection coefficients for the three different probe frequencies indicated in (a) with dashed vertical lines.

Experimental results. The physical device [Fig. 1(b)] consists of a $\lambda/4$-waveguide-resonator cavity capacitively coupled to a transmon with $E_{J\Sigma}/E_C = 58$, flux biased at $\omega_0/(2\pi) = 5.16$ GHz. For the cavity, $\omega_c/(2\pi) = 4.376$ GHz and $\kappa/(2\pi) = 4.0$ MHz. The signals used for spectroscopy and for relaxation measurements are shown in Figs. 1(c) and 1(d).

In Fig. 3(a), we present the measured reflection coefficient Γ as a function of the probe frequency ω_p and the number of cavity quanta N_c at the off-resonant drive frequency $\omega_d/(2\pi) = 4.35$ GHz. The spectrum clearly shows a quantum-to-classical transition and the BS effect, as expected from previous theoretical considerations, and they are well matched by numerical simulations for the Hamiltonian in Eq. (1), generalized to the case of a multilevel transmon [22,33,46] and including the counter-rotating terms. The numerics have converged up to $N_c \approx 100$ for $N = 7$ transmon states. We have also performed a systematic experimental study of the spectrum at various transmon and drive frequencies [33], obtaining similar features to those presented in Fig. 3(a).

In the quantum regime, the transmon behaves as a two-level system (qubit) with only $\hat{\sigma}_z$ coupling to the cavity via a $\hat{a}^\dagger\hat{a}\hat{\sigma}_z$ term [cf. Eq. (2)]. Consequently, the two systems can be addressed separately and, because $[\hat{H},\hat{\sigma}_z] = 0$, the cavity can be used for quantum nondemolition measurements of the qubit population. The higher excited states of the transmon start to contribute to the observed resonance location when

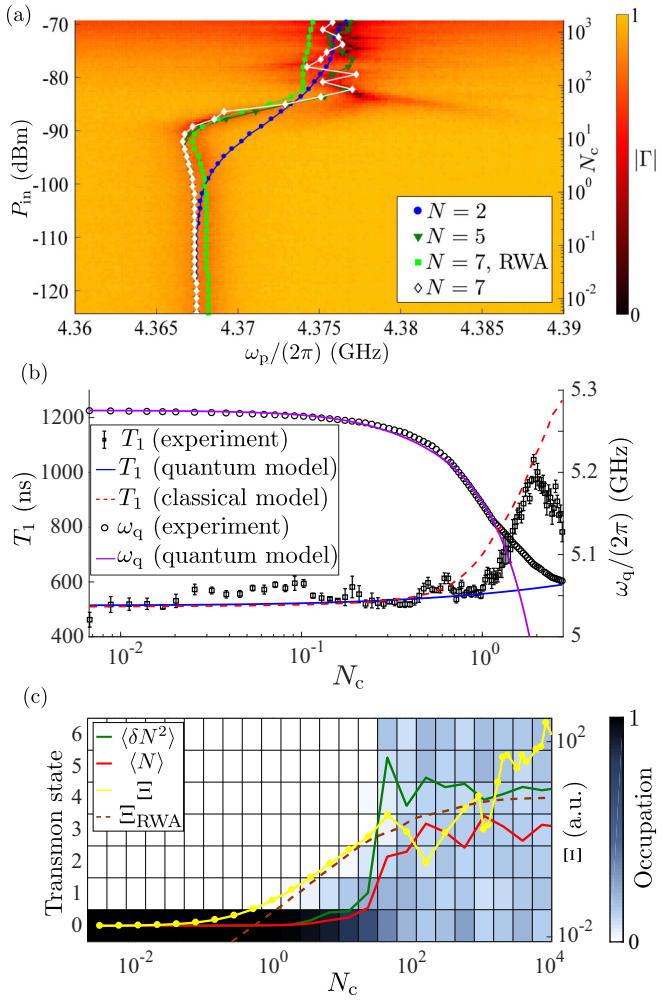

FIG. 3. Frequency renormalization and Bloch-Siegert effect. (a) Measured reflection coefficient $|\Gamma|$ as a function of the probe frequency ω_p and the input power P_{in} at the sample (or equivalent average number of cavity quanta N_c). Numerically calculated resonance frequencies are shown with colored dots for $N = 2,5,7$ transmon states. (b) Measured relaxation time T_1 (left axis) as a function of N_c. On the right axis, we show the ac Stark shifted qubit transition frequency ω_q in the same interval. For $N_c \leqslant 1$, a standard perturbative quantum treatment [47–49] can be used to explain the data (continuous lines), while above these values the increase of T_1 can be modeled using a classical approach [33,50,51]. (c) Quantum-to-classical transition in the driven transmon-cavity system. We show the numerically calculated average transmon state occupation $\langle N \rangle$, occupation number fluctuations $\langle \delta N^2 \rangle$, and the order parameter Ξ as a function of the cavity occupation.

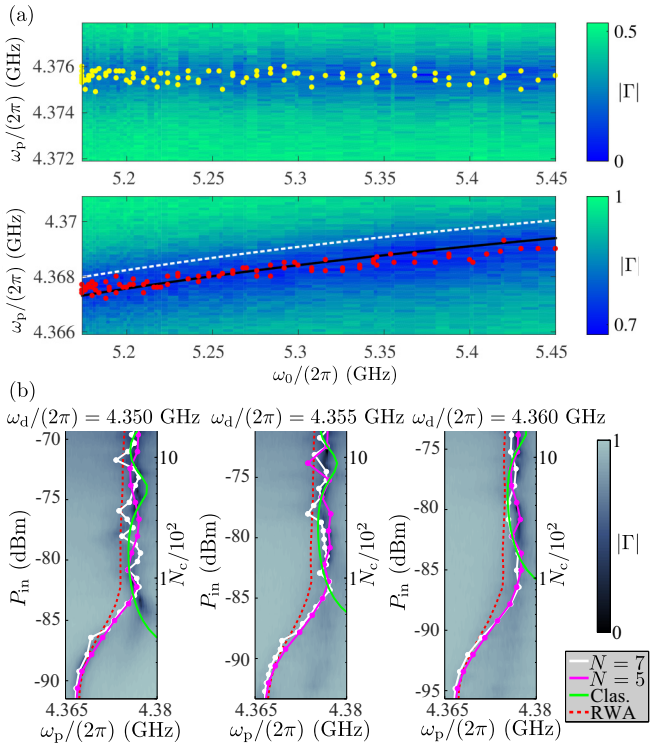

FIG. 4. The Bloch-Siegert effect in the quantum and classical regimes. (a) Measured reflection coefficient $|\Gamma|$ as a function of ω_0 and ω_p, taken at high power (upper panel) and low power (lower panel). The strongest resonance minima extracted from the data are marked with dots. The lower panel demonstrates the vacuum BS shift of $\chi_{BS} = 0.7$ MHz, displayed as the difference between the calculated cavity frequency with only the analytic vacuum Stark shift ($\omega_c - \chi_0$, dashed white line) and with the analytic vacuum BS shift included ($\omega_c - \chi_0 - \chi_{BS}$, solid black line). (b) Bloch-Siegert shift as a function of driving power (corresponding to $N_c = 10$–1650) in the classical regime for $\omega_d/(2\pi) = 4.350$, 4.355, and 4.360 GHz. We show the experimental contour for the reflection coefficient and compare the resonance locations with the classical-approximation formula for ω_+ in Eq. (3) and with the numerical results with $N = 5,7$ ($N = 7$ is calculated also in the RWA).

$N_c \sim 1$, as seen from the deviation between the numerical $N = 2$ and $N = 7$ results in Fig. 2(a). This coincides with the breakdown of the dispersive approximation used in Eq. (2), which is expected to be valid when $N_c \ll N_{crit}$ [47], where $N_{crit} = [(\omega_0 - \omega_c)/(2g)]^2 \approx 30$ for our experimental values.

At the transition and further in the classical regime, the two subsystems become strongly hybridized. In this case, $[\hat{H}, \hat{\sigma}_z] \neq 0$, and therefore the qubit population is no longer conserved. We have observed this effect by performing relaxation measurements: Under continuous constant driving at $\omega_d = 4.366$ GHz [see Fig. 1(d)], we excite the system with a long pulse at the ac Stark shifted transmon frequency and we monitor the response of the cavity after this pulse ends. We extract the relaxation time from fitting the relaxation traces with an exponential [see Fig. 3(b)]. The results show an increase in the relaxation time as the power is ramped up to above a cavity photon number $N_c \approx 1$, coinciding with the onset of the quantum-to-classical transition. In the same power range the qubit frequency decreases according to the standard quantum theory of ac Stark shifted transitions [47–49], which also includes effects caused by the higher transmon energy levels. At about the same number of photons, discrepancies with respect to this model start to appear. A classical theory [33,50,51] which treats the transmon as an anharmonic oscillator provides a good fitting with T_1 up to the power level when the cavity frequency can no longer be taken as constant (about $N_c \approx 2$, after which the measured T_1 drops again).

In Fig. 3(c), we demonstrate that the fluctuations $\langle \delta N^2 \rangle = \langle N^2 \rangle - \langle N \rangle^2$ of the transmon occupation number change

rather abruptly when the drive power is swept over the transition regime. Thus, distinctly from the transition predicted by Carmichael [29], also the transmon becomes a multilevel classical object. In the laboratory frame, we characterize the quantum-to-classical transition by defining a dimensionless order parameter $\Xi = |\langle(\hat{a} + \hat{a}^\dagger)\hat{\Pi}_x\rangle|$, where $\hat{\Pi}_x = \hat{c} + \hat{c}^\dagger$ is the analog of $\hat{\sigma}_x$ and $\hat{c}$ is the annihilation operator for the multilevel transmon [52]. Note that this order parameter includes the correlations between the cavity and the transmon. At low powers the order parameter saturates to a nearly zero value given by $\Xi_{\text{ground}} \approx 2g/(\omega_0 + \omega_c) \approx 10^{-2}$, indicating the quantum regime. As the power increases, the order parameter starts to increase at $N_c \approx 1$ and the fluctuations become large as well. At high enough power (approximately $N_c = 10$), the system enters the classical phase, where a large number of states participate in the dynamics. Interestingly, the BS effect is reproduced by the order parameter, which is seen as the nonmonotonic deviation between the RWA and non-RWA order parameters.

In Fig. 4(a), we further demonstrate the essential difference between the quantum and classical regimes and the role of the Bloch-Siegert shift by analyzing the dependence of the response on the qubit frequency at the two extremes of the drive power. As expected, at very high powers the resonance is located at the bare cavity frequency, irrespective of the qubit frequency. At low drive powers, the resonance location decreases with the qubit frequency, which is characteristic of a vacuum Stark and BS shifted cavity. The inclusion of the vacuum BS shift clearly gives a better fit to the resonance data. We have also studied in more detail the BS effect in the transition region. In addition to numerical results, we can also employ the classical model to calculate the normal modes,

$$\omega_\pm = \sqrt{\frac{\Omega^2 + \omega_c^2}{2} \pm \frac{1}{2}\sqrt{\left[\Omega^2 - \omega_c^2\right]^2 + 16g^2\Omega^2\omega_c/\omega_0}}, \quad (3)$$

where $\Omega^2 = J_0(\sqrt{P_{\text{in}}/P_0})\omega_0^2$, P_{in} is the power fed into the system, and $P_0 = 1.0$ pW. These are obtained by treating the Josephson junction as a classical inductance and by averaging over the drive period [33,53]. In Fig. 4(b), we present the results of experiments at three different drive frequencies. Because the transition occurs at a fixed value $N_c \sim 1$ for all drive frequencies [33], we show the responses in the same interval of cavity quanta, ranging from $N_c = 10$ to 1650. One notices that in all three measurements the BS effect is present. There is very good agreement between the experimental data and the numerics, and also in the high-power region the classical mode ω_+ provides a good match to the data.

To conclude, we have studied a driven-dissipative quantum-to-classical transition in a circuit-QED setup consisting of a transmon coupled to a cavity. The response of the system to a weak probe reveals a clear signature of the Bloch-Siegert shift, which is nonmonotonous in the drive power. Our experiment paves the way toward future experiments of quantum simulations of dissipative phase transitions in one-dimensional circuit-QED lattices.

Discussions with D. Angelakis, E. Thuneberg, M. Silveri, and S. Laine on theory, and M. Sillanpää and J. Pirkkalainen on sample design and fabrication are gratefully acknowledged. We are grateful for the financial support from the Academy of Finland (Projects No. 263457 and No. 135135), the Magnus Ehrnrooth Foundation, the Finnish Cultural Foundation, the Vilho, Yrjö, and Kalle Väisälä Foundation, FQXi, Centre of Quantum Engineering at Aalto University (Project QMET), and the Centres of Excellence LTQ (Project No. 250280), and COMP (Projects No. 251748 and No. 284621). This work used the cryogenic facilities of the Low Temperature Laboratory at OtaNano/Aalto University.

[1] F. Bloch and A. Siegert, Phys. Rev. **57**, 522 (1940).
[2] C. Ciuti and I. Carusotto, Phys. Rev. A **74**, 033811 (2006).
[3] M. Devoret, S. Girvin, and R. Schoelkopf, Ann. Phys. **16**, 767 (2007).
[4] J. Bourassa, J. M. Gambetta, A. A. Abdumalikov, Jr., O. Astafiev, Y. Nakamura, and A. Blais, Phys. Rev. A **80**, 032109 (2009).
[5] G. Günter, A. A. Anappara, J. Hees, A. Sell, G. Biasiol, L. Sorba, S. De Liberato, C. Ciuti, A. Tredicucci, A. Leitenstorfer, and R. Huber, Nature (London) **458**, 178 (2009).
[6] Y. Todorov, A. M. Andrews, R. Colombelli, S. De Liberato, C. Ciuti, P. Klang, G. Strasser, and C. Sirtori, Phys. Rev. Lett. **105**, 196402 (2010).
[7] P. Forn-Díaz, J. Lisenfeld, D. Marcos, J. J. García-Ripoll, E. Solano, C. J. P. M. Harmans, and J. E. Mooij, Phys. Rev. Lett. **105**, 237001 (2010).
[8] T. Niemczyk, F. Deppe, H. Huebl, E. P. Menzel, F. Hocke, M. J. Schwarz, J. J. García-Ripoll, D. Zueco, T. Hümmer, E. Solano, A. Marx, and R. Gross, Nat. Phys. **6**, 772 (2010).
[9] P. Forn-Díaz, J. J. García-Ripoll, B. Peropadre, J.-L. Orgiazzi, M. A. Yurtalan, R. Belyansky, C. M. Wilson, and A. Lupascu, Nat. Phys. **13**, 39 (2017).
[10] F. Yoshihara, T. Fuse, S. Ashhab, K. Kakuyanagi, S. Saito, and K. Semba, Nat. Phys. **13**, 44 (2017).
[11] A. Baust, E. Hoffmann, M. Haeberlein, M. J. Schwarz, P. Eder, J. Goetz, F. Wulschner, E. Xie, L. Zhong, F. Quijandría, D. Zueco, J.-J. García-Ripoll, L. García-Álvarez, G. Romero, E. Solano, K. G. Fedorov, E. P. Menzel, F. Deppe, A. Marx, and R. Gross, Phys. Rev. B **93**, 214501 (2016).
[12] L. S. Bishop, J. M. Chow, J. Koch, A. A. Houck, M. H. Devoret, E. Thuneberg, S. M. Girvin, and R. J. Schoelkopf, Nat. Phys. **5**, 105 (2009).
[13] D. Fregenal, E. Horsdal-Pedersen, L. B. Madsen, M. Forre, J. P. Hansen, and V. N. Ostrovsky, Phys. Rev. A **69**, 031401(R) (2004).
[14] M. Førre, Phys. Rev. A **70**, 013406 (2004).
[15] M. C. Goorden and F. K. Wilhelm, Phys. Rev. B **68**, 012508 (2003).
[16] J. Tuorila, M. Silveri, M. Sillanpää, E. Thuneberg, Yu. Makhlin, and P. Hakonen, Phys. Rev. Lett. **105**, 257003 (2010).
[17] J. Tuorila, M. Silveri, M. Sillanpää, E. Thuneberg, Yu. Makhlin, and P. Hakonen, Supercond. Sci. Technol. **26**, 124001 (2013).

[18] Jian Li, M. P. Silveri, K. S. Kumar, J.-M. Pirkkalainen, A. Vepsäläinen, W. C. Chien, J. Tuorila, M. A. Sillanpää, P. J. Hakonen, E. V. Thuneberg, and G. S. Paraoanu, Nat. Commun. **4**, 1420 (2013).
[19] J. Braumüller, M. Marthaler, A. Schneider, A. Stehli, H. Rotzinger, M. Weides, and A. V. Ustinov, arXiv:1611.08404.
[20] M. J. Hartmann, J. Opt. **18**, 104005 (2016).
[21] C. Noh and D. G. Angelakis, Rep. Prog. Phys. **80**, 016401 (2017).
[22] J. Koch, T. M. Yu, J. Gambetta, A. A. Houck, D. I. Schuster, J. Majer, A. Blais, M. H. Devoret, S. M. Girvin, and R. J. Schoelkopf, Phys. Rev. A **76**, 042319 (2007).
[23] H. Paik, D. I. Schuster, Lev S. Bishop, G. Kirchmair, G. Catelani, A. P. Sears, B. R. Johnson, M. J. Reagor, L. Frunzio, L. I. Glazman, S. M. Girvin, M. H. Devoret, and R. J. Schoelkopf, Phys. Rev. Lett. **107**, 240501 (2011).
[24] M. D. Reed, L. DiCarlo, B. R. Johnson, L. Sun, D. I. Schuster, L. Frunzio, and R. J. Schoelkopf, Phys. Rev. Lett. **105**, 173601 (2010).
[25] M. Boissonneault, J. M. Gambetta, and A. Blais, Phys. Rev. Lett. **105**, 100504 (2010).
[26] L. S. Bishop, E. Ginossar, and S. M. Girvin, Phys. Rev. Lett. **105**, 100505 (2010).
[27] B. Suri, Z. K. Keane, L. S. Bishop, S. Novikov, F. C. Wellstood, and B. S. Palmer, Phys. Rev. A **92**, 063801 (2015).
[28] P. Alsing, D.-S. Guo, and H. J. Carmichael, Phys. Rev. A **45**, 5135 (1992).
[29] H. J. Carmichael, Phys. Rev. X **5**, 031028 (2015).
[30] J. M. Fink, L. Steffen, P. Studer, L. S. Bishop, M. Baur, R. Bianchetti, D. Bozyigit, C. Lang, S. Filipp, P. J. Leek, and A. Wallraff, Phys. Rev. Lett. **105**, 163601 (2010).
[31] J. M. Fink, A. Dombi, A. Vukics, A. Wallraff, and P. Domokos, Phys. Rev. X **7**, 011012 (2017).
[32] J. H. Shirley, Phys. Rev. **138**, B979 (1965); Ya. B. Zeldovich, Zh. Eksp. Teor. Fiz. **51**, 1492 (1966) [Sov. Phys. JETP. **24**, 1006 (1967)].
[33] See Supplemental Material at http://link.aps.org/supplemental/10.1103/PhysRevB.96.020501 for more information on the experimental setup and sample, analytical and numerical models, and additional experimental data at different drive frequencies.
[34] A. Abragam, *Principles of Nuclear Magnetism* (Oxford University Press, Oxford, U.K., 1986).
[35] Z. G. Lü and H. Zheng, Phys. Rev. A **86**, 023831 (2012).
[36] Y. Y. Yan, Z. G. Lü, and H. Zheng, Phys. Rev. A **91**, 053834 (2015).
[37] M. Silveri, J. Tuorila, M. Kemppainen, and E. Thuneberg, Phys. Rev. B **87**, 134505 (2013).
[38] L. D. Landau and E. M. Lifshitz, *Statistical Physics, Part I* (Pergamon, Oxford, U.K., 1980).
[39] R. Blümel, R. Graham, L. Sirko, U. Smilansky, H. Walther, and K. Yamada, Phys. Rev. Lett. **62**, 341 (1989).
[40] R. Blümel, A. Buchleitner, R. Graham, L. Sirko, U. Smilansky, and H. Walther, Phys. Rev. A **44**, 4521 (1991).
[41] M. Grifoni and P. Hänggi, Phys. Rep. **304**, 229 (1998).
[42] S. Gasparinetti, P. Solinas, S. Pugnetti, R. Fazio, and J. P. Pekola, Phys. Rev. Lett. **110**, 150403 (2013).
[43] J. Hausinger and M. Grifoni, Phys. Rev. A **83**, 030301(R) (2011).
[44] J. Hausinger, Ph.D. thesis, Universität Regensburg, 2010.
[45] A. J. Hoffman, S. J. Srinivasan, S. Schmidt, L. Spietz, J. Aumentado, H. E. Türeci, and A. A. Houck, Phys. Rev. Lett. **107**, 053602 (2011).
[46] A. Cottet, Ph.D. thesis, Université Paris VI, 2002.
[47] M. Boissonneault, J. M. Gambetta, and A. Blais, Phys. Rev. A **79**, 013819 (2009).
[48] M. Boissonneault, A. C. Doherty, F. R. Ong, P. Bertet, D. Vion, D. Esteve, and A. Blais, Phys. Rev. A **85**, 022305 (2012).
[49] M. Boissonneault, J. M. Gambetta, and A. Blais, Phys. Rev. A **86**, 022326 (2012).
[50] K. D. Irwin, Appl. Phys. Lett. **66**, 1998 (1995).
[51] K. D. Irwin, Ph.D. thesis, Stanford University, 1995.
[52] L. Bishop, Ph.D. thesis, Yale University, 2010.
[53] O.-P. Saira, M. Zgirski, K. L. Viisanen, D. S. Golubev, and J. P. Pekola, Phys. Rev. Appl. **6**, 024005 (2016).